Analytical Methods

Accepted Manuscript

This article can be cited before page numbers have been issued, to do this please use: Y. Tan, Z. Wang, H. Yin and P. Yu, *Anal. Methods*, 2025, DOI: 10.1039/D5AY00973A.

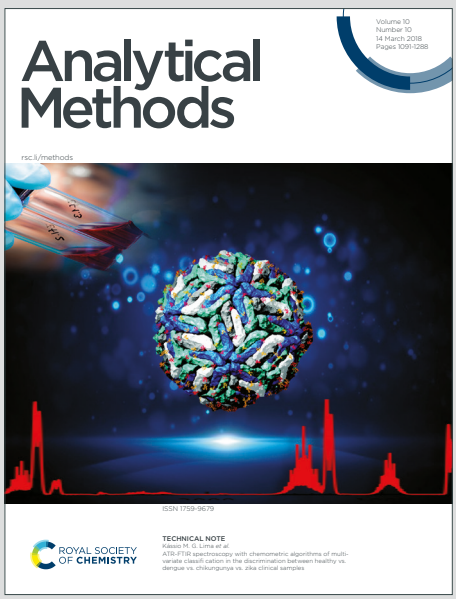

ROYAL SOCIETY OF CHEMISTRY

rsc.li/methods

View Article Online
DOI: 10.1039/D5AY00973A

The electrochemical sensor based on triblock polyadenine-based probe and copper nanoclusters for the robust detection of HPV16 gene

Yan Tan, Zhipeng Wang, Haowen Yin and Peng Yu*

School of Materials Science and Engineering, Xiangtan University, Xiangtan 411105, PR China.

*yupeng@xtu.edu.cn

ORCID ID of Peng Yu: 0000-0002-3195-8049

View Article Online
DOI: 10.1039/D5AY00973A

Abstract

The cervical cancer is the fourth most common cancer among women worldwide. Human papillomavirus type 16 (HPV16) is one of the common biomarkers which cause the cervical cancer. In this work, an electrochemical sensor based on a triblock polyadenine-based probe (TPP) and copper nanoclusters (CuNCs) was constructed for the rapid, sensitive and selective detection of HPV16. The TPP contained the central polyadenine (PolyA) segment and two flanking DNA probes. The middle PolyA segment had a high affinity to the gold electrode surface, leading to the adjustable density of the TPP by the length of PolyA. When the DNA template that mediated the formation of CuNCs was introduced, the DNA template partly hybridized with the two flanking DNA probes of the TPP. A large number of CuNCs were synthesized on the DNA template, producing a big electrochemical impedance signal. When the target DNA (HPV16) was present, it bound to the two flanking DNA probes of the TPP, which resulted in the release of the DNA template from the electrode and produced a small electrochemical impedance signal. The limit of detection (LOD) for the detection of HPV16 was 3.34 pM and the linear range was 10 pM - 10 μM. The designed sensor demonstrated good sensitivity, good selectivity, and satisfied recovery, providing the valuable insights in the cervical cancer prevention and the development of the electrochemical biosensors.

View Article Online
DOI: 10.1039/D5AY00973A

1. Introduction

Human papillomavirus (HPV) is a group of non-enveloped, double-stranded DNA (dsDNA) viruses. It can be categorized into high-risk and low-risk types. High-risk HPV genotypes are the possible reason for the cervical cancer. So far, about 14 types of high-risk HPV genotypes have been reported, and HPV16 and HPV18 are the major high-risk HPV genotypes.[1,2] According to the surveys, the global prevalence of HPV infection varies considerably geographically. The highest prevalence of the HPV infection in women was found in Africa and Asia among the five continents, and particularly in the developing countries with limited medical facilities.[3] Therefore, the development of a simple, rapid, sensitive and cost-effective DNA sensor for detecting the HPV16 gene is crucial for the early diagnosis and prevention of the HPV-related disease.

Currently, the common methods for HPV detection are divided into two kinds. The first is the HPV-specific expressed protein detection method, such as enzyme-linked immunosorbent assay (ELISA) based on the antigen-antibody specific binding. ELISA has low sensitivity and requires a cumbersome cleaning step.[4] The second is the nucleic acid-based assay method, including colorimetry,[5,6] electrochemistry,[7,8] and surface-enhanced Raman sectroscopy.[9,10] Among these methods, the electrochemistry method has a lot of advantages such as simple operation, high sensitivity and low cost.[11] Until now, a large number of nanomaterials have been used to construct the label-free electrochemistry sensors for the sensitive detection of the HPV genetypes.[7,12]

Metal nanoclusters (MNCs) consist of a few to tens of metal atoms, which can be

View Article Online
DOI: 10.1039/D5AY00973A

readily synthesized by DNA template with the special sequence, such as silver nanoclusters (AgNCs) using cytosine (C)-rich DNA template,[13,14] copper nanoclusters (CuNCs) using poly-thymidine [poly(T)] DNA template or poly-(adenine-thymine-thymine-adenine) [poly(AT-TA)] ds-DNA DNA template.[15–18] Among these MNCs, DNA-templated CuNCs are favorable for the various applications due to their mild synthesis conditions, good biocompatibility and inexpensive precursors.[19–21] Moreover, the number and the size of the CuNCs can be regulated by adjusting the DNA sequence.[22] The formation of the CuNCs originates from the clustering of Cu^0, which begins with the chemical reduction of Cu^{II} to Cu^I on the DNA backbones, followed by the conversion of Cu^I to Cu^{II} and Cu^0 due to the disproportionation reaction.[23] The in-situ preparation of CuNCs on DNA backbones is time-saving compared with the ex-situ synthesis preparation process, which lays a substantial basis for its wide applications in the relevant biochemical analyses. For example, the CuNCs were successfully applied to the highly sensitive detection of the targets such as miRNA-122, pyrophosphate and alkaline phosphatase activity and glutathione.[24-26] Therefore, it is meaningful to construct an electrochemical DNA biosensor based on CuNCs for HPV16 detection.

The electrochemical DNA sensors usually utilize the gold-sulfur (Au-S) bond to self-assemble the sulfhydrylated oligonucleotides on the electrode surface. However, the precise control of the orientation and the conformation of the oligonucleotides on the electrode surface and the fine-tuning of the hybridization ability remain challenging.[27,28] In recent years, poly-adenine (PolyA)-based DNA covalent

View Article Online
DOI: 10.1039/D5AY00973A

immobilization strategy has provided the new idea for assembling DNA. Unlike the Au-S bond-dependent immobilization strategy, the binding of PolyA to gold presumably occurs through the coordination mechanism involving the direct interaction of adenine base ring's nitrogen with gold, with the partial contribution from the exocyclic amino group.[29] For example, Li *et al.*[30] reported a novel electrochemical DNA sensor based on a triblock PolyA-based probe (TPP), which achieved the ultra-sensitive and rapid detection of lead ions (Pb^{2+}) by integrating a three-dimensional DNAzyme walker and a strand displacement reaction (SDR). Li *et al.*[31] reported a TPP-based label-free electrochemical DNA sensor for the highly sensitive detection of DNA. Although the breakthrough has been made for the binding of PolyA to the gold surface, there was no electrochemical biosensor that employed TPP for the sensitive detection of HPV16.

In this work, a label-free electrochemical sensor based on TPP and DNA templated CuNCs was constructed for the sensitive detection of HPV16. As shown in Fig. 1, the TPP consisted of a central PolyA fragment and two flanking DNA probes. Unlike the conventional SH-DNA probe, the TPP enabled the probe anchoring through the high affinity of the PolyA segment toward gold, thereby forming a tight biosensing interface on the electrode surface. Such assembling strategy allowed two flanking probes to be immobilized onto the electrode surface at an adjustable distance and in the equal amounts. When the DNA template capable of mediating the formation of CuNCs was introduced into the system, the DNA template partly hybridized with the two flanking probes of the TPP and was thus immobilized on the electrode surface. Subsequently,

View Article Online
DOI: 10.1039/D5AY00973A

numerous CuNCs could be synthesized in situ on the immobilized DNA template, generating a significant impedance signal. However, when HPV16 was present, it displaced the DNA template to preferentially hybridize with the two flanking probes, forming two duplex. This resulted in the release of the DNA template from the electrode surface and the decreased generation of CuNCs, leading to a small impedance signal that was quantitatively related to the amount of HPV16.

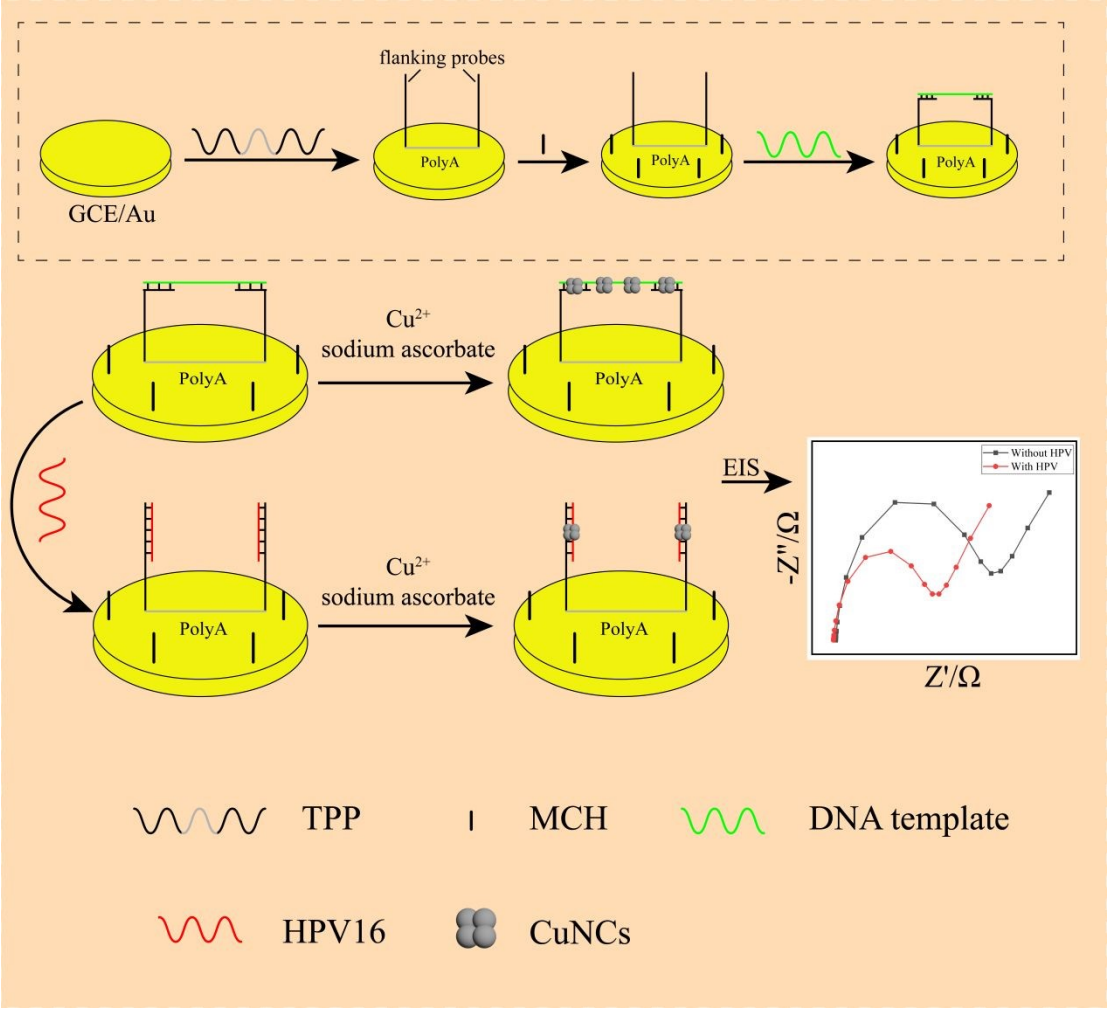

Fig. 1 The construction of the electrochemical sensor based on TPP and CuNCs for HPV16 detection.

2. Experimental

2.1 Reagents and materials

View Article Online
DOI: 10.1039/D5AY00973A

H_2SO_4, $HAuCl_4$, $CuSO_4 \cdot 5H_2O$, ethylenediaminetetraacetic acid (EDTA), NaCl, sodium ascorbate, 6-mercapto-1-hexanol (MCH) were purchased from Shanghai Aladdin Biochemical Technology Co., Ltd. (China). Superior grade fetal bovine serum was purchased from Jiangsu Kaiji Biotechnology Co., Ltd. (China). EDTA buffer solution (pH 7.4) contained 10 mM EDTA and 1 M NaCl. $[Fe(CN)_6]^{3-/4-}$ solution contained 5 mM $K_4[Fe(CN)_6]$, 5 mM $K_3[Fe(CN)_6]$ and 0.1 M KCl. All the solutions were prepared and diluted with the ultrapure water from a Milli-Q (Bedford, USA) ultrapure water system.

All the oligonucleotides used in this study were synthesized by Shanghai Sangon Biological Engineering Technological Co. Ltd. (China) and their sequences are enumerated below:

DNA1: 5'-GCAAAGGCAGCAATGACACACACACAAAAAAAAAACACACACACAGCAGCAATGTTAGCA-3'

DNA2: 5'-GCAAAGGCAGCAATGACACACACACAAAAAAAAAAAAAAAAAAAACACACACACAGCAGCAATGTTAGCA-3'

DNA3 (i.e., TPP): 5'-GCAAAGGCAGCAATGACACACACACAAAAAAAAAAAAAAAAAAAAAAAAAAAAAACACACACACAGCAGCAATGTTAGCA-3'

DNA4: 5'-GCAAAGGCAGCAATGACACACACACAAAAAAAAAAAAAAAAAAAAAAAAAAAAAAAAAACACACACACAGCAGCAATGTTAGCA-3'

DNA template: 5'-CTGCCTTTGCTTTTTTTTTTGCTAACATT-3'

View Article Online
DOI: 10.1039/D5AY00973A

HPV16: 5'-TGCTAACATTGCTGCCTTTGC-3'

HPV18: 5'-GGAATGCTCGAAGGTCGTCT-3'

HPV31: 5'-GGTGAACCGAAAACGGTTGG-3'

HPV51: 5'-TCTGCTGTACAACGCGAAGG-3'

HPV58: 5'-ACAGCTAGGGCACACAATGG-3'

2.2 Instrumentation

The surface morphology of the electrode was obtained by the field emission scanning electron microscopy (FM-SEM, Apreo S, Netherlands). The transmission electron microscopy (TEM) images were obtained using a JEM-2100 transmission electron microscope (Nippon Electron Co., Ltd., Japan). All the electrochemical measurements were performed at a CS310H electrochemical workstation (Wuhan Kesite Instruments Co., Ltd., China). A conventional three-electrode cell was used with a glassy carbon (GC) electrode (diameter = 3 mm) as the working electrode, a platinum wire as the counter electrode and a saturated calomel electrode (SCE) as the reference electrode.

2.3 The preparation of the electrochemical biosensor

The GC electrode was polished using 0.05 μm alumina slurries to obtain a mirror-like surface, followed by the ultrasonication steps in ultrapure water, ethanol, and ultrapure water, respectively. Then the GC elecetrode was immersed in 1 mM H_2SO_4 solution by the potential cycling in the potential between -0.6 and 1.6 V until the cyclic voltammetry characteristic for a clean GC electrode was obtained. After rinsing with ultrapure water, the pretreated GC electrode was immersed in 5 mM $HAuCl_4$ solution

View Article Online
DOI: 10.1039/D5AY00973A

using the constant potential polarization method for the electrodeposition of gold nanoparticles (AuNPs) on the GC electrode surface. After that, the GC/Au electrode was washed with ultrapure water. 15 μL of TPP (1 μM) was placed onto the GC/Au electrode surface and incubated in the dark overnight at room temperature, and the TPP was anchored to the electrode surface to form a triblocked conformation through covalent binding of adenine bases to the AuNPs layer. The obtained GC/Au/TPP electrode was rinsed with ultrapure water and then immersed in 1 mM MCH solution for 30 min to block the uncovered electrode surface. Then, 15 μL of DNA template (1 μM) was dropped on the GC/Au/TPP/MCH electrode surface and incubated at room temperature in the dark for 1 h, and the obtained modified electrode was labeled as GC/Au/TPP/MCH/DNA template.

2.4 The electrochemical measurement

The electrochemical impedance spectroscopy (EIS) and cyclic voltammetry (CV) measurements were both recorded in the $[Fe(CN)_6]^{3-/4-}$ solution. EIS was recorded by applying a frequency range of 10^5 Hz - 10^{-2} Hz and a 10 mV AC amplitude. CV was performed at a scan rate of 100 mV/s over a potential range of -0.2 V ~ 0.6 V.

3. Results and discussion

3.1 The characterization of the developed electrochemical sensor

The morphology of the modified electrode surface after the electrodeposition of AuNPs was characterized by FM-SEM. As shown in Fig. 2A, AuNPs were uniformly dispersed on the sensing interface with an average size of 160 nm. The DNA-templated CuNCs were characterized using TEM. The freshly prepared CuNCs solution was

View Article Online
DOI: 10.1039/D5AY00973A

dropped on an ultrathin carbon film and dried at room temperature. Then the morphology was obtained using TEM. As shown in Fig. 2B, the newly prepared CuNCs were uniformly spherical with a diameter of about 5 nm, indicating the successful synthesis of DNA templated CuNCs.

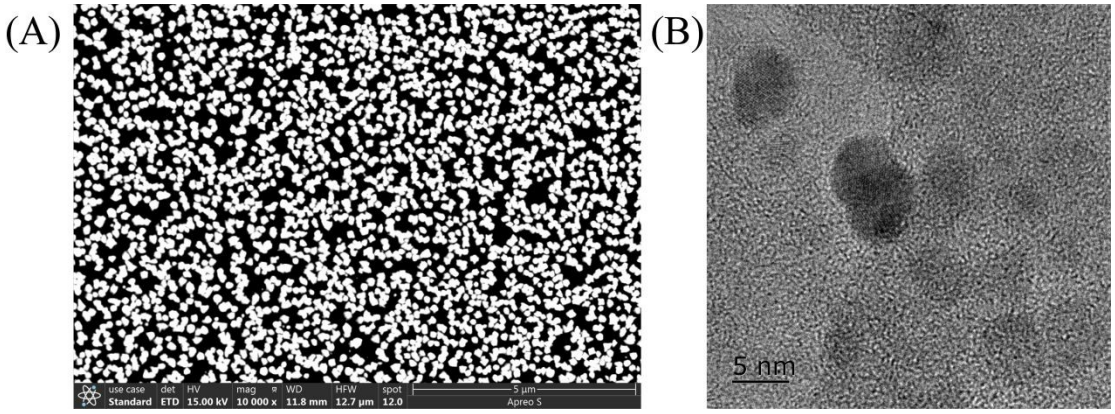

Fig. 2 (A) The SEM image of the GC/Au electrode surface; (B) The TEM image of CuNCs.

Each step in the modification of the electrode was further characterized by EIS and CV. The EIS data were presented in the form of the Nyquist plots and fitted by a equivalent circuit model. The equivalent circuit model includes solution resistance (R_s), electron transfer resistance (R_{et}), capacitance (CPE), and Warburg impedance (Z_w). The R_{et} value is associated with the semicircle at high frequencies in the Nyquist plots, which is the most directive and sensitive parameter in response to the changes at the electrode/solution interface.[32] As shown in Fig. 3A, the Nyquist plot of the GC/Au electrode demonstrated a quick electron transfer with a low R_{et} of 71 Ω, which was almost a straight line (curve a). When the TPP was immobilized on the GC/Au electrode, the R_{et} increased significantly to 722 Ω (curve b). This was due to the mutual repulsion between the negatively charged phosphate skeletons of DNA and the

View Article Online
DOI: 10.1039/D5AY00973A

$[Fe(CN)_6]^{3-/4-}$ probe, which hindered the electron transfer. Subsequently, the GC/Au/TPP electrode was further modified with MCH, which made the electron transfer resistance increasing to 1044 Ω (curve c). The reason was that MCH closed the non-specific sites of the electrode. Then the DNA template was introduced and hybridized with the two flanking probes of TPP to form a double-strand DNA, further increasing the R_{et} to 1175 Ω (curve d). After that, the prepared GC/Au/TPP/MCH/DNA template modified electrode was immersed in a centrifuge tube containing copper sulfate solution, followed by the addition of sodium ascorbate (AA) solution. Under the reducing effect of AA, CuNCs were generated in situ on the flanking probes/DNA template duplex. The CuNCs significantly hindered the electron transfer at the electrode interface, resulting in a significant increase in R_{et} to 2350 Ω (curve e). In the presence of HPV16, HPV16 displaced the DNA template and hybridized with the two flanking probes of TPP to form the new duplexes. The release of DNA template from the electrode surface changed the conformation of TPP and the R_{et} was 1250 Ω (curve f). Compared to the curve d (obtained in the absence of HPV16), the resistance value increased a little bit. Finally, the prepared GC/Au/TPP/MCH/DNA template/HPV16 modified electrode underwent the same procedure to generate the CuNCs on the electrode surface. With a comparison to the GC/Au/TPP/MCH/DNA template/CuNCs electrode (curve e), the GC/Au/TPP/MCH/DNA template/HPV16/CuNCs electrode obtained the decreased number of CuNCs, resulting a small R_{et} of 1546 Ω (curve g) that was notably lower than the 2350 Ω for curve e.

The CV results were shown in Fig. 3B. The $[Fe(CN)_6]^{3-/4-}$ probe exhibited the

View Article Online
DOI: 10.1039/D5AY00973A

quasi-reversible redox peaks with varying peak currents on the different modified electrodes. On the GC/Au electrode surface, the $[Fe(CN)_6]^{3-/4-}$ probe showed the highest oxidation and reduction peak currents (curve a), with a peak current difference of about 87 μA. After assembling the TPP on the GC/Au electrode, both the peak currents decreased slightly (curve b), and the peak current difference dropped to about 73 μA. Further modification with MCH to block the nonspecific adsorption sites led to a further decrease in the peak currents (curve c), with the peak current difference decreasing to approximately 61 μA. The introduction of the DNA template, which hybridized with the TPP to form a negatively charged duplex, enhanced the electrostatic repulsion toward the $[Fe(CN)_6]^{3-/4-}$ probe, resulting in the peak current difference decreasing to 59 μA (curve d). Subsequently, CuNCs were synthesized in situ on this electrode. Their spatial site-blocking effect impeded the electron transfer, yielding a lower peak current difference of 40 μA (curve e). When the target DNA was present, it replaced the DNA template to hybridize with the TPP, further reducing the peak current difference to 54 μA (curve f) compared to the DNA template-only electrode (curve d). Finally, CuNCs were synthesized on the target DNA-incorporated electrode, and the hindering effect of CuNCs further decreased the peak currents (curve g) to a difference of about 48 μA. The CV results were in good consistence with the results of EIS, confirming the successful construction of the electrochemical sensor for HPV16 detection.

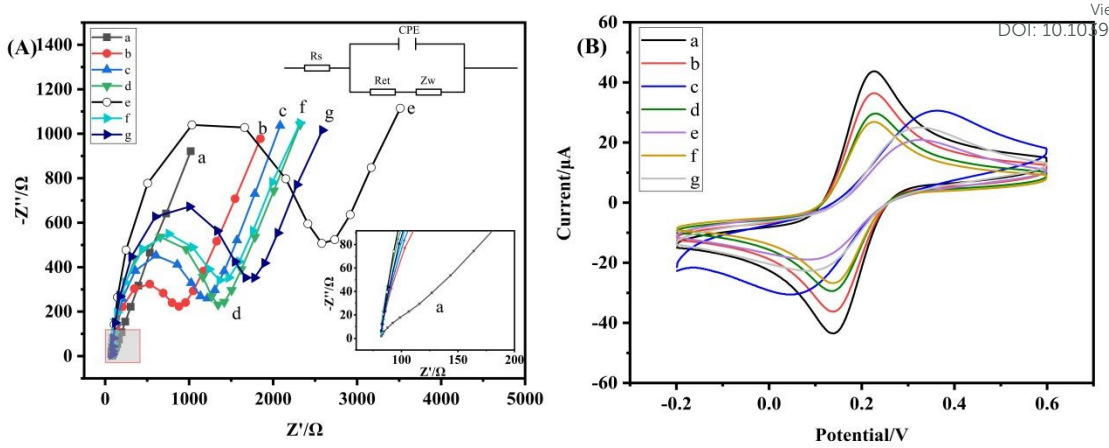

Fig. 3 Nyquist plots (A) and cyclic voltammograms (B) of the different modified electrodes. (a) GC/Au, (b) GC/Au/TPP, (c) GC/Au/TPP/MCH, (d) GC/Au/TPP/MCH/DNA template, (e) GC/Au/TPP/MCH/DNA template/CuNCs, (f) GC/Au/TPP/MCH/DNA template/HPV16, (g) GC/Au/TPP/MCH/DNA template/HPV16/CuNCs.

3.2 The optimization of the length of PolyA segment in TPP

The HPV16 standard solution (1 μM) was employed to optimize the length of PolyA segment (10, 20, 30, and 40 nt) in the TPP, with the corresponding DNA denoted as DNA1, DNA2, DNA3, and DNA4, respectively. As shown in Fig. 4A, as the length of the PolyA segment increased from 10 nt to 30 nt, the impedance signal in the presence of HPV16 gradually decreased while the blank signal gradually increased. The highest signal/noise (S/N) ratio was 13.2 when the length of PolyA segment was 30 nt. (S/N ratio was calculated as follows: $\text{S/N ratio} = \left|\text{average}_{\text{target}} - \text{average}_{\text{blank}}\right| / SD_{\text{blank}}$, where $\text{average}_{\text{target}}$ and $\text{average}_{\text{blank}}$ were the average impedance of the target DNA sample and the blank, respectively. SD_{blank} was the standard deviation of the blank)[33] As can be seen from Fig. 4B, the PolyA with the length of 30 nt matched the length of the DNA template, where the conformational stability was highest at the

View Article Online
DOI: 10.1039/D5AY00973A

electrochemical interface. However, when the length of PolyA increased to 40 nt, the S/N ratio decreased. The results are possibly because that the PolyA sequence was too long, resulting in a low assemble density of the TPP on the electrode surface. Therefore, DNA3 was chosen as the TPP in the subsequent experiments.

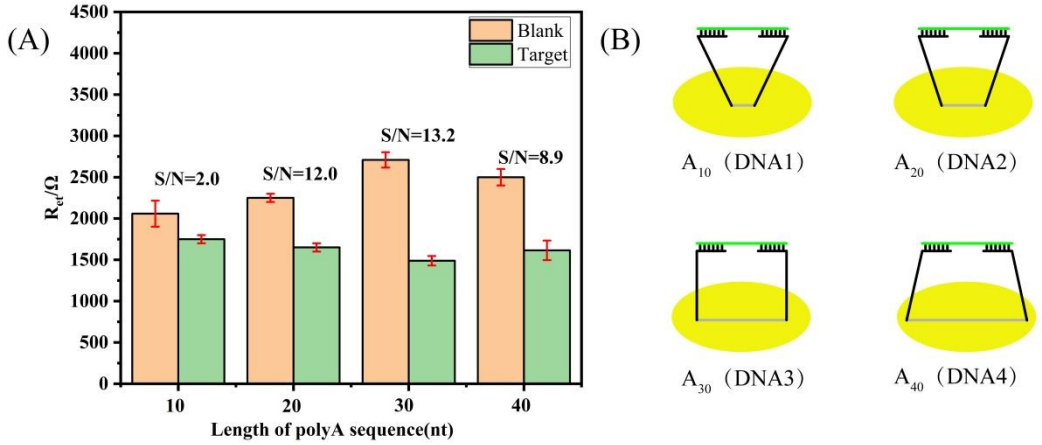

Fig. 4 The effect of the length of PolyA segment in the TPP on the analytical performance (A) and DNA conformation (B).

3.3 The optimization of the reaction parameters

In order to obtain the best performance of the electrochemical sensor for HPV16 detection, several important experimental parameters were optimized. These parameters included the concentration of TPP, the incubation time of MCH, Cu^{2+} concentration and the synthesis time of CuNCs. At first, the concentration of the TPP was first optimized. As shown in Fig. 5A, the highest S/N ratio was 14.1 when the concentration of TPP was 1 μM. Higher concentrations led to the bigger steric hindrance, impairing the immobilization and hybridization of the TPP.[34] Therefore, the optimal concentration of the TPP was 1 μM. MCH blocks the nonspecific adsorption sites on the electrode surface, and the incubation time of MCH is a critical step for constructing the sensor and should be optimized. As shown in Fig. 5B, the S/N ratio

View Article Online
DOI: 10.1039/D5AY00973A

gradually increased with the incubation time of MCH from 10 to 30 min. However, the prolonged incubation beyond 30 min caused a decrease in the S/N ratio. Therefore, the optimal incubation time for MCH was 30 min. CuNCs was responsible for the electrochemical readout, so the concentration of Cu^{2+} was optimized. As shown in Fig. 5C, the S/N ratio gradually increased as the Cu^{2+} concentration increased from 1 mM to 10 mM. However, when the concentration of Cu^{2+} exceeded 10 mM, the S/N ratio gradually decreased. The highest S/N ratio was obtained at 10 mM of Cu^{2+}. Therefore, the optimal concentration of Cu^{2+} was 10 mM. The synthesis time of CuNCs was another important parameter. As shown in Fig. 5D, the S/N ratio gradually increased with increasing the synthesis time for CuNCs, reached a maximum at 20 min, and then gradually decreased with further increasing the reaction time. Therefore, the optimal synthesis time for CuNCs was 20 min.

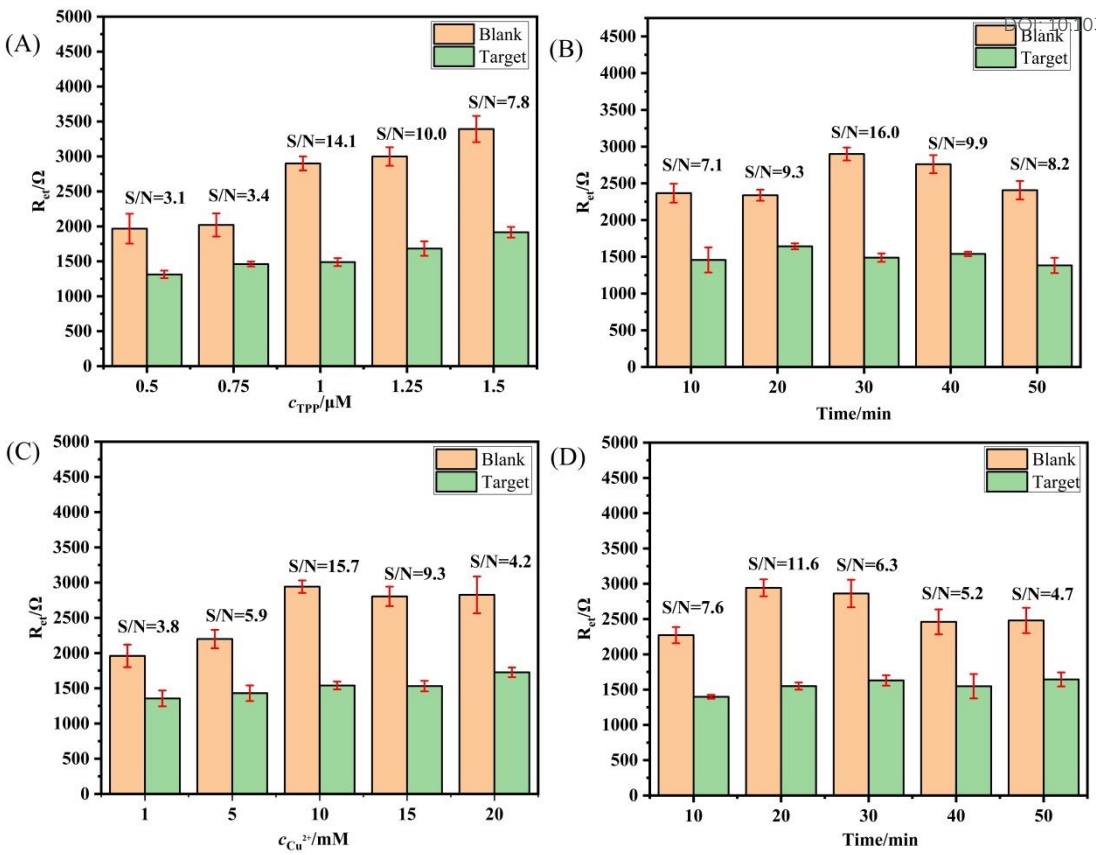

Fig. 5 The effects of c_{TPP} (A), the incubation time for MCH (B), $c_{Cu^{2+}}$ (C) and the synthesis time of CuNCs (D) on the electrochemical signal.

3.4 The analytical performance of the electrochemical sensor for HPV16 determination

Under the optimized conditions, the different concentrations of HPV16 gene were detected using the developed electrochemical sensor, and the results were shown in Fig. 6A. The impedance value gradually decreased when the HPV16 concentration increased from 10 pM to 10 μM. Fig. 6B showed that the linear range for HPV16 gene detection was 10 pM - 10 μM, and the linear equation was R_{et} = -219.02 lg$c$ + 1849.97, R^2 = 0.99. The limit of detection (LOD) of the constructed sensing platform was calculated to be 3.34 pM based on the equation: LOD = 3σ/S (where the standard deviation of the blank sample set is denoted as σ and the slope of the fitted line in Fig.

View Article Online
DOI: 10.1039/D5AY00973A

6B is denoted as S).[7] As shown in Table 1, the analytical performance of the electrochemical sensor developed in this work was compared with other reported sensors for HPV16 detection. The linear range of the developed sensor in this work was much wider and the LOD was lower or comparable towards other sensors. Although this work has achieved good analytical performance in the detection of HPV16 DNA, there are still some improvements needed including the long-term stability, the reversibility of the sensor, the scalability and the real-world deployment, which are something those we hope to explore in further work.

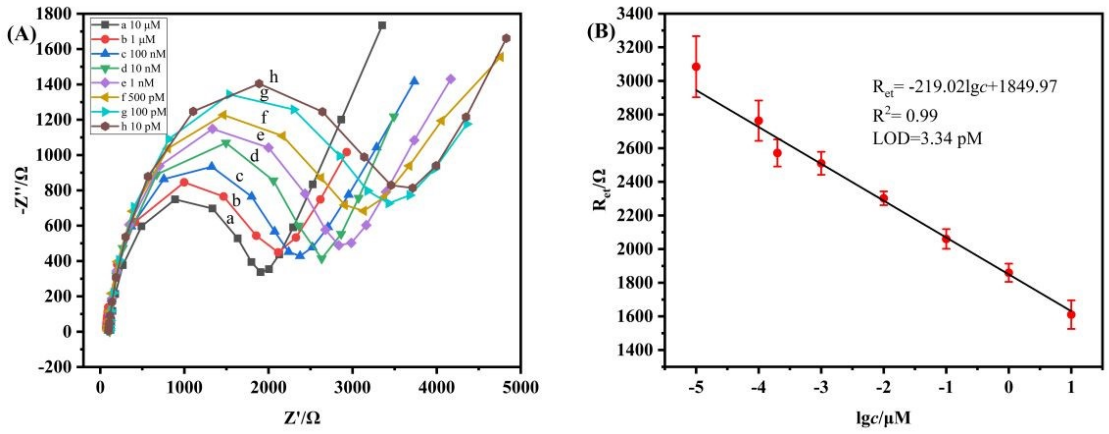

Fig. 6 (A) The Nyquist plots of the electrochemical sensor in the presence of the different concentrations of HPV16 gene; (B) The calibration curve of the resistance versus the logarithmic of HPV16 concentration.

Table 1 The comparison of the analytical performance of the various methods for HPV16 DNA detection

Technique	Probe	Linear range	LOD	Ref.
fluorescence	CdTe quantum dots	0.1 nM - 40 nM	62 pM	35
microfluidic	DNA	0.05 nM - 5.1 nM	10.5 pM	36
microfluidic	copper oxide nanoparticle	5 nM - 100 nM	1 nM	37

View Article Online
DOI: 10.1039/D5AY00973A

electrochemistry	DNA	0.005 nM - 5 nM	18.5 pM	38
electrochemistry	carbon nanotubes and graphene oxide supported ionic liquid	8.5 nM - 10.7 μM	1.3 nM	39
electrochemistry	HRP-tetramethylbenzidine	0.1 nM - 10 nM	220 pM	40
electrochemistry	porous reduced graphene oxide-molybdenum disulfide	3.5 pM - 35.3 pM	1.75 pM	41
electrochemistry	CuNCs	10 pM - 10 μM	3.34 pM	this work

3.5 Selectivity

Selectivity is one of the most important criteria to judge the performance of the sensor, which means being able to to distinguish the analyte from other interferent species in the sample. The specificity of the proposed DNA sensor was performed by analyzing four HPV genetypes (HPV18, HPV31, HPV51 and HPV58) using the same experimental procedure. Fig. 7 clearly shows that with a comparison to HPV16, the other HPV genetypes produced the larger impedance signals even at concentrations 100 times higher than HPV16. The results indicate that the proposed sensor shows the satisfactory selectivity toward HPV16.

View Article Online
DOI: 10.1039/D5AY00973A

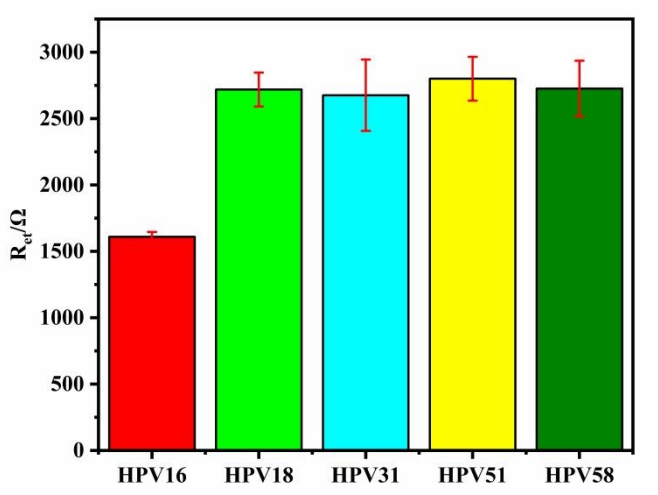

Fig. 7 The selectivity of the sensor for HPV16 detection. The concentration of HPV16 was 1 μM while the concentration of other HPV genetypes was 100 μM.

3.6 Recovery investigation

The suitability of the developed electrochemical sensor was investigated by the recovery test using the 20-fold diluted bovine serum as the real sample. HPV16 was added into the 20-fold diluted bovine serum with different concentrations (1, 10, 100, and 1000 nM), and the results are shown in Table 2. The recoveries of HPV16 ranged between 93.8% to 99.0%. The relative standard deviation (RSD) of the recoveries fluctuated between 2.6% to 6.2%. These results indicate that the constructed electrochemical sensor could be used for the detection of HPV16 in the real sample.

Table 2 The recoveries of HPV16 in the 20-fold diluted bovine serum samples (n=3)

Sample no.	added (nM)	found (nM)	RSD (%)	recovery (%)
1	1	0.99	5.0	99.0
2	10	9.56	2.6	95.6
3	100	97.23	3.8	97.2

View Article Online
DOI: 10.1039/D5AY00973A

4	1000	938.6	6.2	93.8

4. Conclusions

In this work, a label-free electrochemical sensor based on TPP and DNA-templated CuNCs was developed for the highly sensitive detection of HPV16. The PolyA segment in the TPP played a key role in assembling DNA on the electrode with a high affinity. The length of the PolyA segment could induce the conformation change of TPP and thus affect the electron transfer on the electrode. When the PolyA length was 30 nt, the sensor obtained the highest S/N ratio. Moreover, CuNCs were introduced into the sensor to provide the electrochemical signal for the sensitive detection of HPV16. The important parameters affecting the analytical performance were optimized, including the TPP concentration, MCH incubation time, Cu^{2+} concentration, and CuNCs synthesis time. Under the optimized conditions, the developed electrochemical sensor showed a low LOD of 3.34 pM for HPV16 detection and a wide linear range of 10 pM - 10 μM. In addition, the sensor also performed good selectivity and satisfied recovery. This work not only provided a new highly sensitive detection method for the early screening of HPV16, but also expanded the application of TPP in the electrochemical sensing. Furthermore, the multiplexed detection could be achieved by changing the sequences of the flanking probes of TPP. The developed sensor could also be integrated into a portable device by combining the microfluidic technology and the disposable electrode.

Author contributions

Y.T. and P.Y. conceived and designed the experiments. Z.W. performed the

View Article Online
DOI: 10.1039/D5AY00973A

348 experiments. Y.T., Z.W., H.Y. and P.Y. analyzed the data. Y.T. and P.Y. wrote the
349 paper. All authors reviewed and commented on the manuscript.

350 Conflicts of interest

351 There are no conflicts to declare.

352 Acknowledgements

353 This research was funded by the Research Foundation for PhD of Xiangtan
354 University [grant number 18QDZ03].

355

View Article Online
DOI: 10.1039/D5AY00973A

Notes and references

1 H. B. Baghi, P. S. Aghbash, R. Rasizadeh, V. Poortahmasebi and F. Alinez had, *Explor. Res. Hypothesis Med.*, 2024, **9**, 115–127.

2 C. Han, W. Huang, M. Ye, R. Zou, J. Lan, J. Chen, J. Jiang, H. Wang, L. Xia, J. Luo, D. Li, J. Geng, Z. Wang and J. Huang, *Front. Public Health*, 2023, **11**, 1225652.

3 L. Su, H. Peng and X. He, *Clin. Exp. Obstet. Gynecol.*, 2023, **50**, 48.

4 Z. Q. Toh, L. He, C. Chen, A. Huang, F. M. Russell, S. M. Garland, R. R eyburn, T. Ratu, E. Tuivaga, I. H. Frazer, E. K. Mulholland and P. V. Licc iardi, *Front. Immunol.*, 2020, **11**, 585768.

5 J. Chen, M. Wang, C. Zhou, J. Zhang and X. Su, *Talanta*, 2022, **247**, 1235 54.

6 D. Liang, W. You, Y. Yu, Y. Geng, F. Lv and B. Zhang, *RSC Adv.*, 2015, **5**, 27571–27575.

7 Y. Yang, Y. Liao, Y. Qing, H. Li and J. Du, *Sensors*, 2023, **23**, 7380.

8 T.-R. Rashid, D.-T. Phan and G.-S. Chung, *Sens. Actuators B Chem.*, 2014, **193**, 869–876.

9 A. Su, Y. Liu, X. Cao, W. Xu, C. Liang and S. Xu, *Sens. Actuators B Ch em.*, 2022, **369**, 132295.

10 J. Bansal, I. Singh, P. K. Bhatnagar and P. C. Mathur, *J. Biosci. Bioeng.*, 2 013, **115**, 438–441.

11 Y. Zhao, J. Xiang, H. Cheng, X. Liu and F. Li, *Biosens. Bioelectron.*, 2021, **194**, 113581.

12 K. Y. P. S. Avelino, L. S. Oliveira, N. Lucena-Silva, C. P. De Melo, C. A. S. Andrade and M. D. L. Oliveira, *J. Pharm. Biomed. Anal.*, 2020, **185**, 1 13249.

13 A. Latorre and Á. Somoza, *ChemBioChem*, 2012, **13**, 951–958.

14 C. Yang, K. Shi, B. Dou, Y. Xiang, Y. Chai and R. Yuan, *ACS Appl. Mat er. Interfaces*, 2015, **7**, 1188–1193.

15 Z. Mao, Z. Qing, T. Qing, F. Xu, L. Wen, X. He, D. He, H. Shi and K. Wang, *Anal. Chem.*, 2015, **87**, 7454–7460.

16 S. Lv, R. Shi, R. Yan and P. Miao, *J. Electroanal. Chem.*, 2023, **946**, 1177 49.

17 X. Jia, J. Li, L. Han, J. Ren, X. Yang and E. Wang, *ACS Nano*, 2012, **6**,

View Article Online
DOI: 10.1039/D5AY00973A

3311–3317.

18 A. Rotaru, S. Dutta, E. Jentzsch, K. Gothelf and A. Mokhir, *Angew. Chem. Int. Ed.*, 2010, **49**, 5665–5667.

19 Z. Qing, X. He, D. He, K. Wang, F. Xu, T. Qing and X. Yang, *Angew. Chem. Int. Ed.*, 2013, **52**, 9719–9722.

20 Z. Zhou, Y. Du and S. Dong, *Anal. Chem.*, 2011, **83**, 5122–5127.

21 M. Chen, X. Xiang, K. Wu, H. He, H. Chen and C. Ma, *Sensors*, 2017, **17**, 2684.

22 Q. Song, Y. Shi, D. He, S. Xu and J. Ouyang, *Chem. – Eur. J.*, 2015, **21**, 2417–2422.

23 T. Lei, T. Huang, T. Wang, P. Yu, T. Qing and B. Nie, *New J. Chem.*, 2020, **44**, 17296–17301.

24 Y. Qing, H. Fang, Y. Yang, Y. Liao, H. Li, Z. Wang and J. Du, *Biosensors*, 2023, **13**, 854.

25 L. Yao, X. Li, H. Li, Z. Liao, C. Xie, G. Ning, Y. Wu and Y. Wang, *J. Fluoresc.*, 2022, **32**, 1949–1957.

26 S. M. Ragab, M. M. Aboelnga, E. A. Moawed, R. R. El Sadda and G. M. Khairy, Spectrochim. Acta. A. Mol. Biomol. Spectrosc., 2025, 328, 125465.

27 J. Zhang, L. Wang, D. Pan, S. Song and C. Fan, *Chem Commun*, 2007, 1154–1156.

28 R. Lao, S. Song, H. Wu, L. Wang, Z. Zhang, L. He and C. Fan, *Anal. Chem.*, 2005, **77**, 6475–6480.

29 K. M. Koo, A. A. I. Sina, L. G. Carrascosa, M. J. A. Shiddiky and M. Trau, *Anal. Methods*, 2015, **7**, 7042–7054.

30 D. Li, Y. Liu, Y. Li, S. Li and Y. Tang, *Sens. Actuators B Chem.*, 2024, **401**, 134909.

31 L. Li and Z. Chen, *Bioelectrochemistry*, 2023, **153**, 108494.

32 D. Zhang, Y. Wang, X. Jin, Q. Xiao and S. Huang, *Electroanalysis*, 2022, **34**, 1001–1011.

33 L. Li and Z. Chen, *Bioelectrochemistry*, 2023, **153**, 108494.

34 L. Li, L. Wang, Q. Xu, L. Xu, W. Liang, Y. Li, M. Ding, A. Aldalbahi, Z. Ge, L. Wang, J. Yan, N. Lu, J. Li, Y. Wen and G. Liu, *ACS Appl. Mater. Interfaces*, 2018, **10**, 6895–6903.

35 X. Jiang, C. Yin, M. Wu, S. Cao, N. Niu and L. Chen, *Sens. Actuators B*

View Article Online
DOI: 10.1039/D5AY00973A

Chem., 2024, **403**, 135128.

36 A. C. Soares, J. C. Soares, V. C. Rodrigues, H. D. M. Follmann, L. M. R. B. Arantes, A. C. Carvalho, M. E. Melendez, J. H. T. G. Fregnani, R. M. Reis, A. L. Carvalho and O. N. Oliveira, *ACS Appl. Mater. Interfaces*, 2018, **10**, 36757–36763.

37 Z. Yang, C. Yi, S. Lv, Y. Sheng, W. Wen, X. Zhang and S. Wang, *Sens. Actuators B Chem.*, 2019, **285**, 326–332.

38 J. C. Soares, M. E. Melendez, A. C. Soares, L. M. R. B. Arantes, V. D. C. Rodrigues, A. L. Carvalho, R. M. Reis, L. H. C. Mattoso and O. N. Oliveira Jr, *Mater. Chem. Front.*, 2020, **4**, 3258–3266.

39 L. Farzin, S. Sadjadi, M. Shamsipur and S. Sheibani, *J. Pharm. Biomed. Anal.*, 2020, **179**, 112989.

40 L. Civit, A. Fragoso, S. Hölters, M. Dürst and C. K. O'Sullivan, *Anal. Chim. Acta*, 2012, **715**, 93–98.

41 F. Chekin, K. Bagga, P. Subramanian, R. Jijie, S. K. Singh, S. Kurungot, R. Boukherroub and S. Szunerits, *Sens. Actuators B Chem.*, 2018, **262**, 991–1000.

View Article Online
DOI: 10.1039/D5AY00973A

Data Availability Statement

The authors confirm that the data supporting the findings of this study are available within the article [and/or its supplementary materials].

Authors: Yan Tan, Zhipeng Wang, Haowen Yin and Peng Yu